Earth and Planetary Science Letters 432 (2015) 73–83

Contents lists available at ScienceDirect

Earth and Planetary Science Letters

www.elsevier.com/locate/epsl

Faulting and erosion in the Argentine Precordillera during changes in subduction regime: Reconciling bedrock cooling and detrital records

Julie C. Fosdick [a,*], Barbara Carrapa [b], Gustavo Ortíz [c]

[a] Department of Geological Sciences, Indiana University, 1001 East 10th Street, Bloomington, IN 47405, USA
[b] Department of Geosciences, University of Arizona, 1040 East 4th Street, Tucson, AZ 85721, USA
[c] Centro de Investigaciones de la Geósfera y la Biósfera (CIGEOBIO), Facultad de Ciencias Exactas, Físicas y Naturales, Universidad Nacional de San Juan, Meglioli 1160 Sur, San Juan, Argentina

ARTICLE INFO

Article history:
Received 6 May 2015
Received in revised form 18 September 2015
Accepted 26 September 2015
Available online 3 November 2015
Editor: A. Yin

Keywords:
Argentine Precordillera
fold-and-thrust belt
thermochronology
foreland basin

ABSTRACT

The Argentine Precordillera is an archetypal retroarc fold-and-thrust belt that records tectonics associated with changing subduction regimes. The interactions between exhumation and faulting in the Precordillera were investigated using apatite and zircon (U–Th–Sm)/He and apatite fission track thermochronometry from the Precordillera and adjacent geologic domains. Inverse modeling of thermal histories constrains eastward in-sequence rock cooling associated with deformation and erosion from 18 to 2 Ma across the Central Precordillera tracking thrusting during this time. The youngest AHe ages (5–2 Ma) and highest erosion rates are located in the eastern and western extremities of the Precordillera and indicate that recent denudation is concentrated at its structural boundaries. Moreover, synchronous rapid Pliocene cooling of the Frontal Cordillera, Eastern Precordillera, and Sierra del Valle Fértil was coeval with initiation of basement-involved faulting in the foreland. Detrital zircon U–Pb geochronology from the ca. 16–8.1 Ma Bermejo foreland basin strata suggests fluvial connectivity westward beyond the Frontal Cordillera to the Main Cordillera and Coast Range followed by an important shift in sediment provenance at ca. 10 Ma. At this time, we suggest that a substantial decrease in Permo-Triassic igneous sources in the Frontal Cordillera and concurrent increase in recycled zircons signatures of Paleozoic strata are best explained by uplift and erosion of the Precordillera during widening of the thrust-belt. Bedrock thermochronology and modeling indicate a 2–6 Myr lag time between faulting-related cooling in the hinterland and the detrital record of deformation in the foreland basin, suggesting that for tectonically active semi-arid settings, bedrock cooling may be more sensitive to onset of faulting. We suggest that high erosion rates in the Frontal Cordillera and Eastern Precordillera are associated with increased interplate coupling during shallowing of the subducting Nazca plate that may concentrate stress along weak structural boundaries of the Precordillera.

1. Introduction

The physiography of contractional mountain belts is largely controlled by the interaction between lithospheric thickening and the erosional removal and redistribution of mass from steepened highlands to adjacent basins (e.g., Beaumont et al., 1992). One of the most influential advances in our knowledge of the tectonic development of mountain belts is that erosion can influence the location of strain and thus the overall geometry and outward growth of orogenic belts (e.g., Koons and Kirby, 2007). At the same time, foreland basin sedimentary archives remain invaluable records of changes in erosion of source areas, and the time and rates of deformation and exhumation. Deciphering causal relationships and potential feedbacks between faulting and erosion thereby rely on robust temporal constraints and our understanding of time lags between deformation, rock uplift, cooling and erosion, and sedimentation at 10^6 yr timescales (e.g., Burbank, 2002; Lock and Willett, 2008).

In thin-skinned retroarc fold-and-thrust belts, the structural development is modulated largely by the mechanical behavior of the basal decollément and modification of the surface slope by accretion or erosion (Davis et al., 1983). However, in retroarc settings characterized by complex subduction zone dynamics such as shallow subduction, both the deformational and exhumational behavior may be more complex. For instance, shallow subduction

* Corresponding author.
E-mail address: jfosdick@indiana.edu (J.C. Fosdick).

http://dx.doi.org/10.1016/j.epsl.2015.09.041
0012-821X/

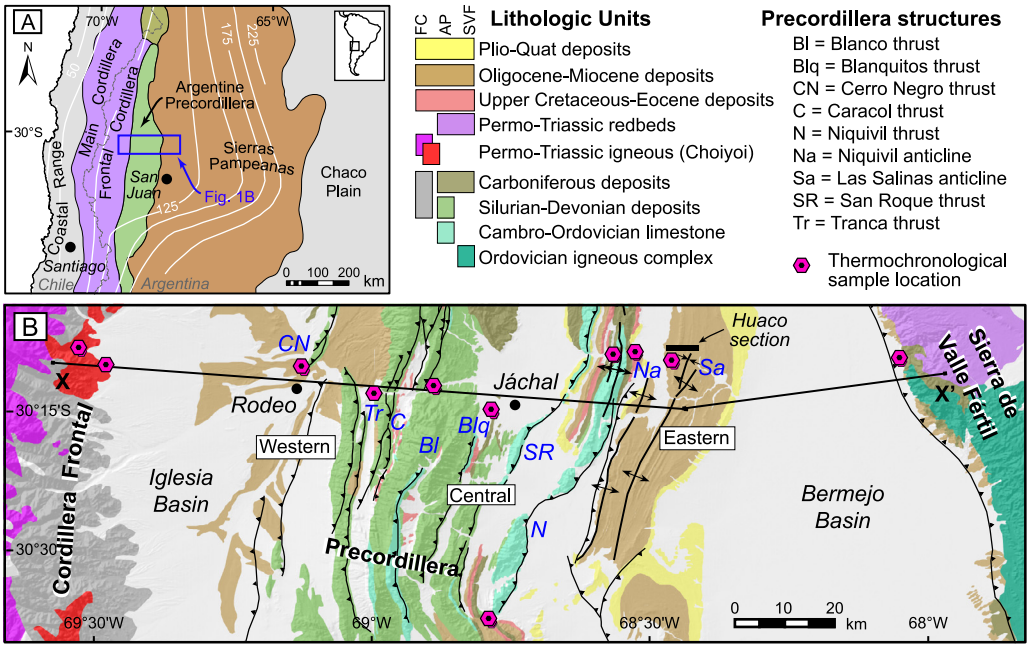

Fig. 1. (A) Tectonic setting of the Argentine Precordillera and adjacent provinces in the southern Central Andes. White lines denote depth in km to the Wadati-Benioff zone (Cahill and Isacks, 1992). (B) Geologic map of the study area in the Precordillera with Cenozoic thrust faults and thermochronology sample locations. Black bar labeled Huaco section denotes location of detrital geochronology sample suite. Fault nomenclature modified after Jordan et al. (2001). Cross-section X–X′ is depicted in Fig. 2. Geology and cross-section modified from Zapata and Allmendinger (1996), Furque et al. (2003), and new mapping from this study. FC = Frontal Cordillera, AP = Argentine Precordillera, and SVF = Sierra de Valle Fértil.

of oceanic lithosphere may increase interplate coupling between the subducting slab and the overriding plate by long distance transmission of compressional stress across the foreland (e.g., Gutscher et al., 2000). Reactivation of basement heterogeneities (e.g., Hilley et al., 2005; Ramos et al., 2002) in flat slab settings may also promote reverse faulting and uplift of crystalline basement, such as in the Laramide ranges of North America and the Sierras Pampeanas of Argentina (Jordan and Allmendinger, 1986; Ramos et al., 2002). In contrast to relatively well-studied faulting in basement-cored uplift blocks, the response of the thin-skinned thrust belt domain to changes in subduction geometry is unclear: how do exhumation rates vary across different structural styles? Do extinct hinterland structures become reactivated during shallow subduction? Do detrital and bedrock cooling records resolve synchronous deformational histories across the thrust belt?

The Pampean flat slab segment of the southern Central Andes (between 27°S and 33°30′S) is the ideal place to investigate the impact of shallow subduction and upper plate orogenic processes on deformation and erosion of retroarc fold-and-thrust belts (Fig. 1, Table 1). The Precordillera is an important player in Andean tectonics because it records the structural and exhumational response to a changing tectonic regime during the transition from Oligocene–Miocene steep subduction to Late Miocene–Pliocene flat subduction and thick-skinned deformation (Jordan and Allmendinger, 1986; Jordan et al., 1993). With its well-preserved intermontane and foreland basin stratigraphy, the Precordillera is often cited as one of the best dated thrust belts in the world (Fig. 2). However, less is known about its exhumational history, and how the kinematic evolution of the individual thrust sheets during shallow slab subduction has impacted erosion. To evaluate the exhumational response of the Precordillera to changes in plate interactions and to investigate relationships between faulting and erosion across different structural styles, we performed low-temperature thermochronology, thermal modeling, and detrital zircon geochronology in the Precordillera and adjacent provinces.

2. Tectonic setting

The southern Central Andes is subdivided into several morphotectonic domains based on structural style, physiography, and foreland basin configuration (Ramos, 2009). Between 28°S and 33°S, the Pampean (Chilean) flat slab segment of the Nazca Plate subducts subhorizontally beneath South America (Cahill and Isacks, 1992). The Andean orogen from west to east consists of the Coastal Cordillera, the Main and Frontal Cordilleras, the Argentina Precordillera, and the Pampean ranges, with intervening Neogene foreland basins (Fig. 1A). Shallowing of the Pampean flat slab has been attributed to southward propagating subduction of the aseismic Juan Fernández Ridge in the Nazca Plate beginning ca. 18 Ma (Ramos et al., 2002; Yañez et al., 2001) and is reflected by a cessation of arc magmatism and initiation of basement-involved deformation in the Sierras Pampeanas (Jordan and Allmendinger, 1986; Kay et al., 2005). The initiation of shallow subduction at the latitude of the study area (30°S) is constrained by magmatic and sedimentary records at ca. 10–5 Ma (Jordan et al., 1993; Kay et al., 2005).

The Argentina Precordillera is a north-south trending, ~50 km wide orogenic wedge involving Paleozoic through late Cenozoic sedimentary rocks uplifted in six major east-verging thrust sheets (Fig. 1B) (Allmendinger et al., 1990; Jordan et al., 1993; Ramos et al., 2002). These Andean structures have resulted in substantial shortening and offset of Cenozoic basin infill (Allmendinger and Judge, 2014), although debate exists regarding the extent to which some of the Precordillera deformation is related to early Paleozoic events later overprinted by Cenozoic high-angle faulting (e.g., Alonso et al., 2014; Alvarez-Marrón et al., 2006). The Precordillera is subdivided into three structural domains. The Western and Central Precordillera are characterized by highly deformed Paleozoic sedimentary rocks and intermontane Neogene basins (Allmendinger and Judge, 2014; Furque et al., 2003; Jordan et al., 1993). The Eastern Precordillera consists of a thick-skinned triangle zone developed in crystalline basement with Pliocene syntec-

Table 1
Thermochronology and detrital geochronology sample locations.

Sample name	Latitude (°S)	Longitude (°W)	Elevation (m)	Formation/lithology and location	ZHe	AHe	AFT	DZ
FC01	−30.14146	−69.52620	3073	Permian granite; Frontal FC hangingwall	•	•		
FC03	−30.16638	−69.48009	2858	Permian granite; Frontal FC hangingwall			•	
JT01	−30.15287	−68.56559	1046	Silurian argillite; Niquivil thrust hangingwall		•		
JT07	−30.20958	−68.88860	1378	Silurian argillite; Blanco thrust hangingwall	•	•		
JT10	−30.21938	−68.99572	1508	Silurian argillite; Tranca thrust footwall	•	•		
JT12	−30.25276	−68.78512	1295	Permian sandstone; Blanquitos thrust hangingwall		•		
JT15	−30.17494	−69.12577	1563	Silurian argillite; Western AP; Cerro Negro	•	•		
SVF01	−30.15897	−68.05082	857	Carboniferous sandstone; SVF thrust hangingwall	•	•		
RH10	−30.14859	−68.52666	1024	Vallecito Fm (Oligocene); Niquivil thrust footwall		•		
RF11	−30.62882	−68.78916	1383	Cuculí Fm (Miocene); Río Francia		•		
HC01	−30.16201	−68.46432	966	Quebrada del Jarillal Fm (Miocene); Las Salinas				•
HC02	−30.16406	−68.46072	1053	Quebrada del Jarillal Fm (Miocene); Las Salinas		•		•
HC04	−30.16332	−68.45181	972	Huachipampa Fm (Miocene); Las Salinas anticline		•		•
HC06	−30.16606	−68.44112	943	Quebrada del Cura Fm (Miocene); Las Salinas				•
HC07	−30.15923	−68.43294	924	Río Jáchal Fm (Miocene); Las Salinas anticline		•	•	

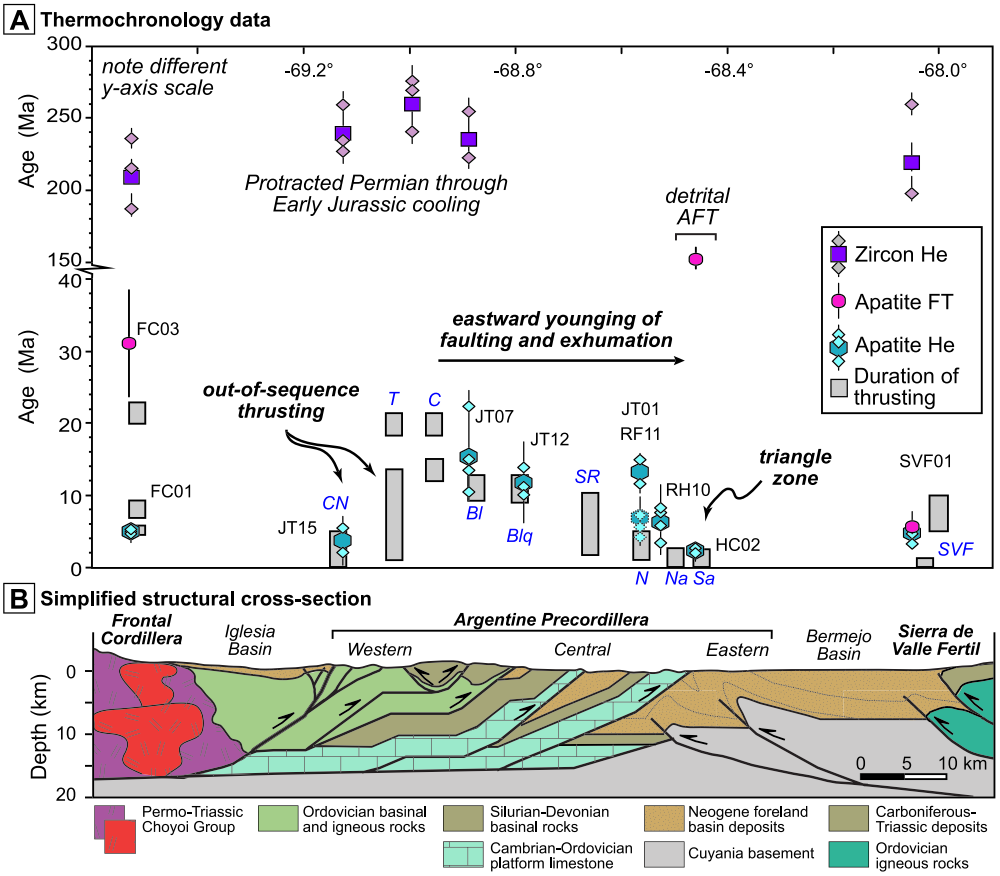

Fig. 2. (A) Thermochronometric data from the Precordillera and adjacent provinces. Diamonds show single-grain zircon and apatite (U–Th)/He dates, with weighted mean ages for each sample shown by hexagons (apatite) and squares (zircon). AFT ages are shown by pink circles. Published chronology of Cenozoic thrust motion (gray boxes) is based on Jordan et al. (2001) and Allmendinger and Judge (2014). Refer to Fig. 1 for legend and cross-section information. (For interpretation of the references to color in this figure legend, the reader is referred to the web version of this article.)

tonic growth strata that are well imaged by seismic-reflection data (Vergés et al., 2007; Zapata and Allmendinger, 1996). East of the Precordillera, basement rocks overlain by Paleozoic and Mesozoic strata are exposed in the west-verging Sierra de Valle Fértil in the Sierras Pampeanas Province (Fig. 1B).

The chronology of deformation in the Precordillera at the latitude of Jáchal is based on the sedimentation history in the genetically linked Bermejo retroarc foreland and Iglesia piggyback basins (Allmendinger and Judge, 2014; Jordan et al., 2001, 1993). Well-dated changes in sediment provenance, depositional facies, subsidence rates, and crosscutting relationships (e.g., Beer et al., 1990; Johnson et al., 1986; Jordan et al., 2001, 1993) depict an in-sequence deformational history beginning ca. 20 Ma in the Western Precordillera, with Pliocene reactivation of faulting in the Iglesia basin and basement uplift along the Eastern Precordillera as evidenced by displaced Pliocene sedimentary rocks and subsurface imaging of faults (Beer et al., 1990; Zapata and Allmendinger, 1996). Most of the crustal shortening in the Andes at this latitude is accommodated by the Western and Central Precordillera. Recent revisions to the kinematic restorations of structural cross-sections of the Precordillera indicate $\sim 90 \pm 21$ km of upper crustal shortening since 13 Ma, most of which is interpreted to have accrued

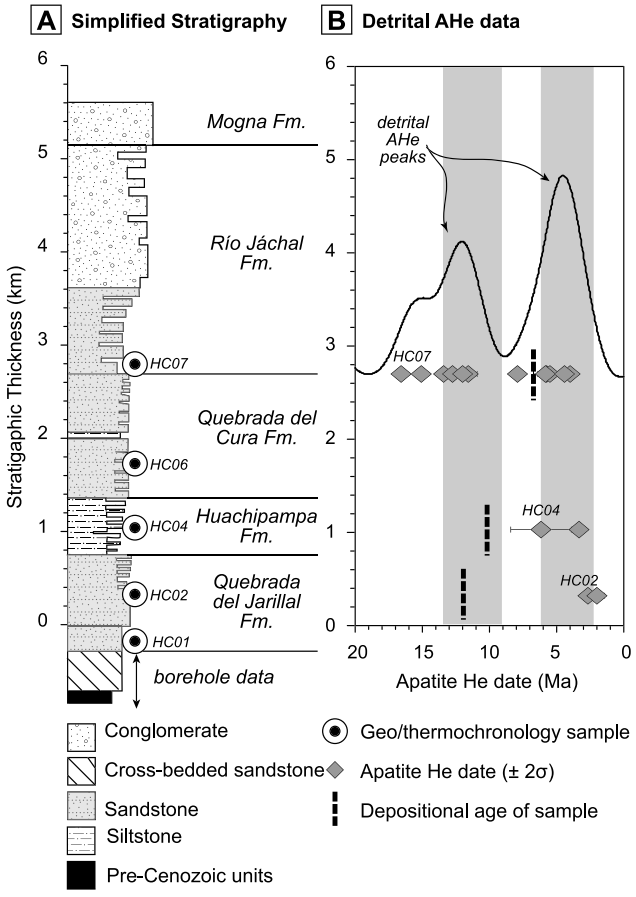

Fig. 3. A) Generalized stratigraphy of the Huaco section (after Jordan et al., 2001) showing detrital thermochronology and geochronology sample positions. B) Detrital apatite (U–Th)/He thermochronometric data from HC02, HC04, and HC07. Samples exhibit down-section increase in the degree of thermal resetting, resulting in AHe dates younger than depositional age. HC02 yields fully reset AHe dates that record Pliocene unroofing of the Huaco section.

between 12 and 9 Ma (Allmendinger and Judge, 2014). Paleoaltimetry data of the intermontane basins within the Precordillera indicate a southward transition in the magnitude of surface uplift along the Precordillera, and present-day elevations at the latitude of the Iglesia Basin were attained prior to 9 Ma (Hoke et al., 2014a), consistent with the crustal shortening history (Jordan et al., 2001, 1993). Pliocene deformation is evident in both the Iglesia basin and the Eastern Precordillera triangle zone (Zapata and Allmendinger, 1996) (Fig. 2). Active deformation is expressed by extensive crustal seismicity (Alvarado et al., 2007), including several historic large magnitude ($M > 6.0$) earthquakes in the San Juan Province of Argentina.

The Neogene Bermejo Basin stratigraphy is well-exposed in the Sierra de Huaco near Jáchal (Fig. 2) as a result of Pliocene deformation and uplift of the basin infill (Zapata and Allmendinger, 1996). The Huaco section is one of the thickest accumulations of Neogene sediments in the area, and consists of conglomerate, sandstone, siltstone, and rare air-fall volcanic tuff, deposited in a semi-arid continental setting (Fig. 3) (Johnson et al., 1986; Jordan et al., 1993). Sedimentological studies of these deposits suggest an evolution in a semi-arid depositional setting from a through-going, low-relief braided fluvial system to an ephemeral distributary channel and alluvial fan system (Johnson et al., 1986). This relatively complete section spans ca. 16–2 Ma and affords the opportunity to track provenance unroofing patterns during this time.

3. Methods and results

3.1. (U–Th–Sm)/He thermochronology

Low-temperature thermochronological techniques are well-suited to investigate the thermal history of thrust sheets and sediments during orogenesis (e.g., Lock and Willett, 2008; Reiners and Brandon, 2006). The (U–Th)/He thermochronology method is based upon thermally controlled retention of ^{4}He gas produced during the decay of radioactive ^{238}U, ^{235}U, ^{232}Th and ^{147}Sm in accessory minerals such as apatite and zircon (e.g., Ehlers and Farley, 2003). At low temperature, He diffusivities are sufficiently low that He is retained within the host mineral, whereas at high temperatures, He is diffusively lost from the crystal. The temperature transition over which this occurs for ^{4}He is called the partial retention zone and ranges from ~160–200 °C for zircon and ~55–80 °C for apatite (Reiners and Brandon, 2006 and references therein). Analytical methods, references, and data are reported in the Supplementary Information.

We performed (U–Th–Sm)/He analysis (He thermochronology) on five zircon samples (14 single grains) and 10 apatite samples (37 single grains) collected from the Precordillera and adjacent provinces. Our sampling strategy targets the ramp-flat reset zone above the hangingwall (Lock and Willett, 2008) or proximal to the fault tip in the footwall block to maximize detection of thermal histories related to faulting. Sample lithologies include Permian granite from the Frontal Cordillera, metamorphosed Silurian–Carboniferous sandstone units exposed in the Precordillera and Sierra de Valle Fértil, and synorogenic Oligocene–Miocene subarkoses and litharenites from the Bermejo Basin.

Zircon He thermochronology (ZHe) samples yield single grain dates between 187 Ma and 275 Ma (Fig. 2A). All bedrock samples show relatively poor intrasample reproducibility based on analytical precision (for $n = 3$ grains per sample), although they are still likely within real uncertainty of each other taking into account the uncertainty of F_T correction for small grains. ZHe dates do not exhibit a strong correlation to eU, although there is an inverse correlation between grain size and ZHe date (Fig. A-1).

Apatite He thermochronology (AHe) dates from the AP and intervening foreland deposits range between 58 Ma and 2 Ma, with all Paleozoic thrust sheet samples falling exclusively between 20 Ma and 2 Ma (Fig. 2). Single-grain dates from the Precordillera display reasonably good reproducibility within samples, from which we calculate weighted mean ages (Fig. 2). Weighted mean AHe ages display a broad bell-shaped distribution across the AP, with young ages (5–4 Ma) at Cerro Negro, north of Rodeo, in the Iglesia Basin, the Frontal Cordillera, and in the Sierra de Valle Fértil. Spanning the Central Precordillera, ages progressively young eastward from ca. 14 Ma to 6 Ma (Fig. 2). The youngest AHe ages (2 Ma) are centered in the Eastern Precordillera.

Detrital AHe data from the exhumed Bermejo Basin strata show variable post-depositional resetting as a function of stratigraphic position and burial depth (Fig. 3). Oligocene–Middle Miocene strata yield invariant AHe dates within each sample, all of which are younger than depositional age. In contrast, Upper Miocene samples yield detrital AHe dates ($n = 18$) that mostly predate depositional age indicating a lower degree of thermal resetting post deposition (Fig. 3B). Sample HC07 from the Upper Miocene Río Jáchal Formation contains prominent detrital signatures at 5 Ma and 13 Ma, with lesser AHe dates between 42–55 Ma (Fig. 3B). Positive correlation between AHe dates and effective uranium concentration (eU) may indicate that burial heating was sufficient to partially reset the low eU apatites (Fig. A-1).

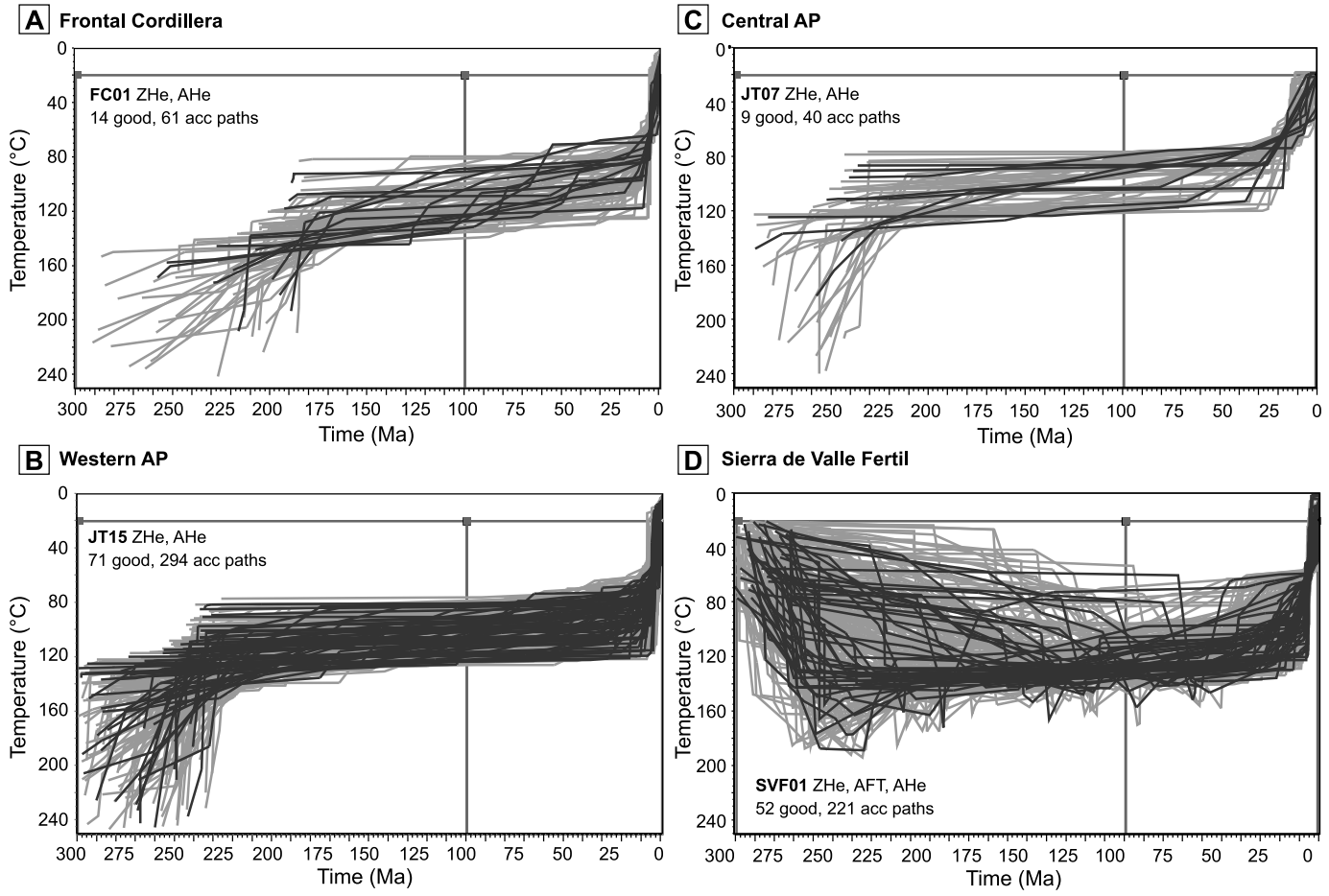

Fig. 4. Inverse modeling results for (A) FC01 Frontal Cordillera, (B) JF15 Cerro Negro, (C) JT07 Central AP, and (D) SVF01 Sierra de Valle Fértil. The results are displayed as temperature–time (T–t) paths for good (black) and acceptable (gray) fit histories. Each model attempted 100,000 T–t paths. Dark gray squares represent the imposed T–t constraints.

3.2. Apatite fission track thermochronology

Our AHe results are supplemented by apatite fission track thermochronology (AFT) data that broadly constrain regional cooling across the study area (Fig. 2). The fission track method is based on the accumulation of linear damage trails in the crystal lattice formed by the spontaneous fission decay of ^{238}U. In apatite, these tracks are completely annealed, or erased, at temperatures above ~120 °C, and retained below ~60 °C (Green et al., 1989), a temperature range termed the partial annealing zone. Analytical methods, references, and data are reported in the Supplementary Information. AFT was attempted on all samples, although low apatite yield, combined with low U concentration, produced limited results. Sample FC03 from a Permian granite in the Colangüil batholith in the Frontal Cordillera yields a pooled AFT age of 31.2 ± 7.7 Ma. In the Eastern AP, sample HC07 shows mixed AFT ages with a central age of 152.3 ± 5.9 Ma. We interpret these limited results as detrital ages and suggest that the basin infill has not been sufficiently buried to reset AFT ages. Farther west in the Sierra de Valle Fértil hangingwall foothills, sandstone from the Carboniferous Guandacol Fm. yields an AFT age of 5.8 ± 0.8 Ma, which is within uncertainty of its AHe date (Fig. 2B).

3.3. Inverse modeling of thermochronometric data and interpretations

We inverse modeled the T–t histories of key samples with AHe, AFT and ZHe data using the HeFTy modeling program (Ketcham, 2005) to evaluate plausible cooling histories for the Precordillera and adjacent provinces (Fig. 4). All models with older ZHe dates are characterized by late Paleozoic – early Mesozoic cooling to below ~140 °C, followed by extended residence between ~140–80 °C until Cenozoic time (Fig. 4). Model results for the Blanco Thrust (JT07) in the Central Precordillera are consistent with rapid cooling through the AHe PRZ at ca. 16–14 Ma followed by slow cooling to present-day. In contrast, the hangingwall of the Cerro Negro thrust in the Western Precordillera (JT15) underwent later rapid cooling at ca. 8–2 Ma (Fig. 4). Cooling paths for the Colangüil pluton in the Frontal Cordillera (FC01) show onset of initial cooling at ca. 10–8 Ma followed by rapid Pliocene cooling to present day. Lastly, model results from the Sierra de Valle Fértil hangingwall thrust block (SVF01) depict Paleozoic–Mesozoic post-depositional burial heating to temperatures within and above the AFT PRZ, followed by rapid cooling since ca. 10–8 Ma. Taken together, the inverse modeled T–t histories depict overlapping Late Miocene cooling through the AHe PRZ for rocks sampled from the Frontal Cordillera, Eastern Precordillera, and Sierra de Valle Fértil. Notably, the thermochronometric data for the Central Precordillera samples satisfy an earlier Middle Miocene cooling history (Fig. 4).

3.4. Detrital zircon U–Pb geochronology

In order to assess changes in sediment provenance during deformation of the Precordillera and foreland basin evolution, we performed LA-ICPMS U–Pb geochronology on four detrital zircon samples from Miocene strata in the Huaco section (Johnson et al., 1986; Jordan et al., 2001). Sandstone samples were collected from

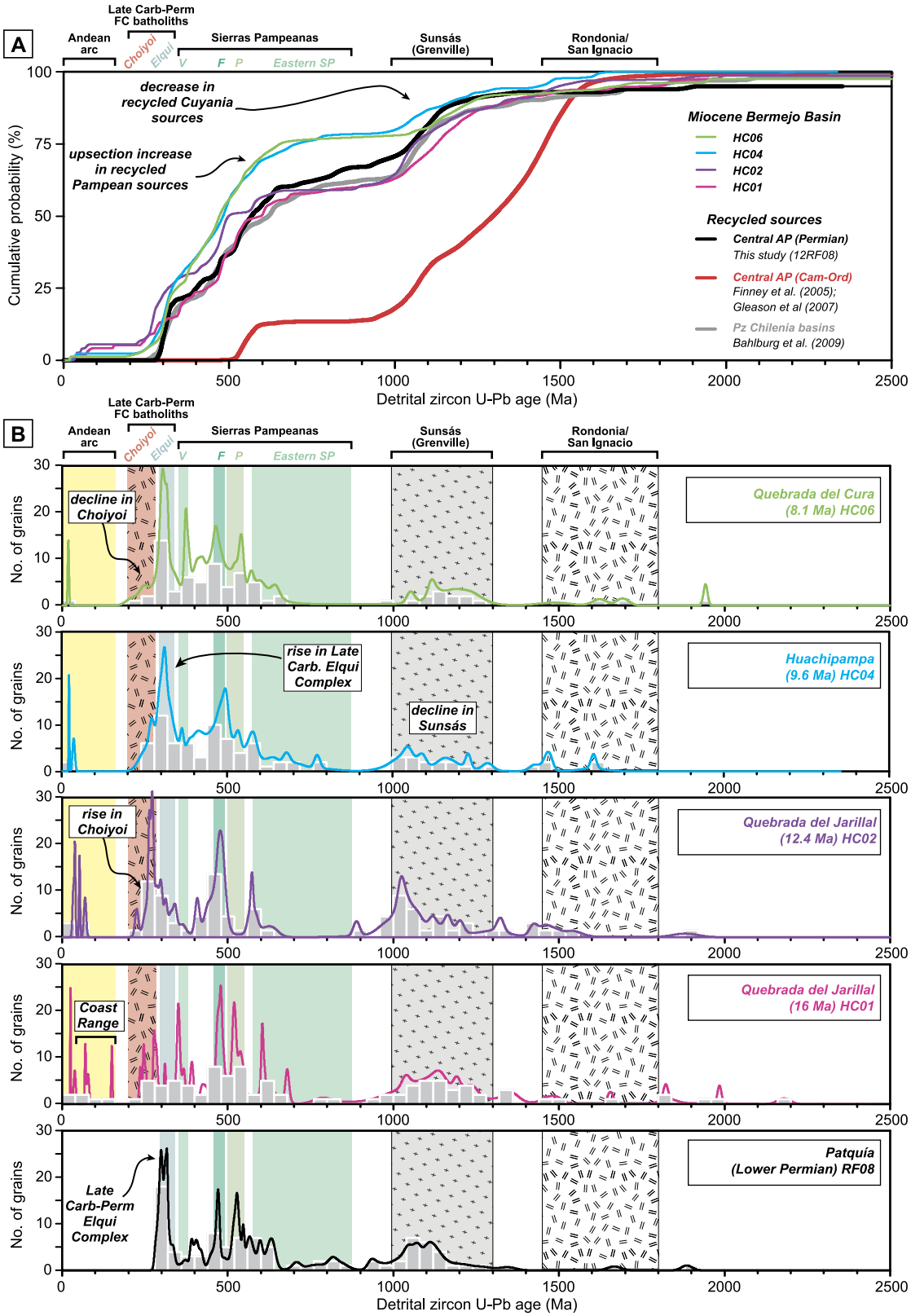

Fig. 5. Detrital zircon geochronology data from the Bermejo Basin and Precordillera. A) Cumulative probability distribution of detrital samples shown in comparison to recycled Paleozoic sediment sources. F = Famatinian arc; P = Pampean arc. B) Relative probability distributions and histograms for Huaco section. Note similarity between samples from the Quebrada del Jarillal Fm. (pink and purple) and the substantial change in zircon signatures in the Huachipampa Fm. (HC04) between 12.4 and 9.6 Ma (blue and green), when the P–T Choiyoi zircons decrease and the Carboniferous zircons rise in large abundance. (For interpretation of the references to color in this figure legend, the reader is referred to the web version of this article.)

well-characterized and dated (by magnetostratigraphy) levels at ca. 16.0 Ma, 12.4 Ma, 9.6 Ma, and 8.1 Ma (Fig. 3) (after Johnson et al., 1986, with revised geomagnetic timescale of Cande and Kent, 1995). We also collected detrital zircon U–Pb data from the Permian Patquía Formation (RF08) to assess the recycled provenance signature from strata exposed in the Central Precordillera. Detrital zircon U–Pb results are displayed as cumulative probability distributions and histograms with corresponding probability distributions in ascending stratigraphic order (Fig. 5). Analytical methods, Concordia diagrams, and analytical data are reported in the Supplementary Information.

Detrital zircon U-Pb ages from the ca. 16 Ma lower Quebrada del Jarillal Fm. (HC01) range from 13 to 2180 Ma ($n = 99$). Prominent zircon age groups occur between 850–1420 Ma, 460–575 Ma, and 240–450 Ma, with fewer grains between 70–150 Ma and 13–14 Ma.

The ca. 12.4 Ma upper Quebrada del Jarillal Fm. (HC02) yields detrital zircon U–Pb ages between 34 and 2596 Ma ($n = 74$), with age populations between 900–1375 Ma, 400–515 Ma, 250–325 Ma, and 34–40 Ma. Key age peaks are 37 Ma, 272 Ma, 478 Ma, 1025 Ma, and 1120 Ma.

Detrital zircon U–Pb results from the ca. 9.6 Ma Huachipampa Formation (HC04) range from 10 to 1606 Ma ($n = 92$), with the youngest resolved age peak overlapping in time with depositional age. Broadly defined age groups are 10–36 Ma, 215–770 Ma, and 930–1295 Ma. Prominent age peaks occur at 270 Ma, 310 Ma, 415 Ma, 495 Ma, and 1046 Ma.

The ca. 8.1 Ma Quebrada del Cura Fm. yields detrital zircon U–Pb ages from 13 to 3383 Ma ($n = 80$). Most zircon ages fall between 220–695 Ma and 1020–1310 Ma, with prominent age peaks at 303 Ma, 316 Ma, 464 Ma, 540 Ma, and 1188 Ma.

Detrital zircons from the Permian Patquía Fm. (RF08) range in age from 282 to 3354 Ma ($n = 99$), with most zircons between 345–280, 435–660, and 1275–920 Ma. Prominent age peaks occur at 299 Ma, 316 Ma, 528 Ma, 1071 and 1111 Ma.

4. Discussion

4.1. Structural influence on thrust belt erosional behavior

Thermochronological results from the Precordillera highlight important temporal correlations between deformation and erosion during orogenic wedge development, as well as nominal constraints on the magnitude of pre-Andean exhumation. The highest temperature thermochronometer yields an old (>187 Ma) suite of zircon He dates from across the study area (Fig. 2). Thermal modeling of these data requires the present-day erosional level of this region – spanning the Frontal Cordillera foothills, Precordillera, and Sierra de Valle Fértil – to have resided at temperatures below He closure in zircon (~180 °C) and corresponding ~8–9 km closure depth since early Mesozoic time (Fig. 4). Zircon He dates overlap in time with the development of the Permo-Triassic Choiyoi magmatism and intraplate extension across Chile and Argentina (Mpodozis and Kay, 1992). We therefore interpret these data to reflect regional bedrock cooling associated with Late Paleozoic – Early Mesozoic intraplate extension of the crust, consistent with the tectonic history of the region (e.g., Ramos, 2009).

In contrast to the pre-Cenozoic ZHe results, Oligocene through Pliocene dates from the lower temperature AHe and AFT thermochronometers constrain >2–3 km of erosion during concurrent deformation in the Andean retroarc region. AFT data, though sparse, corroborate a general eastward shift in the locus of erosion since Oligocene time (Fig. 2). AHe dates young eastward across the Central Precordillera from 16–14 Ma and broadly overlap in space and time with the onset of faulting (Allmendinger and Judge, 2014; Jordan et al., 2001). Taken together, our findings indicate that the most rapid denudation occurs in areas of most recent faulting. Notably, the structural margins of the Precordillera have undergone the most recent bedrock cooling compared to its internal domain (Fig. 4). Our analysis resolves a pronounced signal of cooling and inferred erosion beginning at 8 Ma along the Cerro Negro thrust in the Iglesia piggyback basin, coeval with out-of-sequence sinistral transpressional deformation during orogenic construction (Alvarez-Marrón et al., 2006; Beer et al., 1990) (Fig. 2).

Young AHe dates are also observed in the Frontal Cordillera foothills on the western edge of the Iglesia Basin, where the reset 5 Ma AHe date from Permian granite indicate Pliocene exhumation coeval with flat-slab subduction. Although no active thrust fault is mapped or imaged along the base of the Frontal Cordillera at this latitude (Allmendinger et al., 1990; Beer et al., 1990), the 5 Ma cooling ages and associated relatively high erosion rates likely reflect the removal of thick sedimentary cover in the Iglesia Basin once the Río Jáchal incised through the Precordillera, as suggested by Beer et al. (1990). We interpret the Oligocene AFT age from the Frontal Cordillera to likely reflect exhumation and cooling related to incipient deformation during early stages of Bermejo foreland basin evolution. In contrast, the tectonically active Frontal Cordillera farther south between 33–34°S yields unreset AHe ages suggestive of limited (<2–3 km) exhumation during faulting (Hoke et al., 2014b). These findings together with our data from the Iglesia Basin, suggest that the magnitude and rates of erosion are not only controlled by along-strike changes in faulting history, but also by the amount of sediment burial and subsequent removal during reorganization of drainage basins.

In the Eastern Precordillera, contractional deformation and uplift of ~3 km during growth of the Salinas Anticline, in the thick-skinned triangle zone occurred after ca. 2.6 Ma, based on the depositional age of syngrowth strata (Zapata and Allmendinger, 1996). Correspondingly, ca. 2 Ma AHe ages from Middle Miocene strata sampled directly over the anticline (HC02) indicate rapid post-depositional burial heating followed by unroofing during deformation (Fig. 2). Farther east in the Sierra de Valle Fértil, rapid cooling through the ~120–60 °C temperature window suggests high Pliocene cooling rates (Fig. 4) associated with faulting and erosion of the Sierra de Valle Fértil hangingwall block (Jordan et al., 2001; Ortíz et al., in press).

We compare the deformation history with erosion rates inferred from AHe thermochronometric cooling ages following the method of Willet and Brandon (2013), using a geothermal gradient of $20 \pm 5\,^{\circ}\mathrm{C\,km^{-1}}$ and accounting for $\pm 2\sigma$ uncertainty in age. Bedrock cooling paths suggest onset of cooling between 18–14 Ma for the Central Precordillera (Fig. 4), with moderate ($0.33–0.49\ \mathrm{mm\,yr^{-1}}$) rates of erosion since then (Fig. 6). In contrast, the structural margins of the Precordillera have undergone more recent rock cooling and deeper exhumation, with high erosion rates ($1.52–2.58\ \mathrm{mm\,yr^{-1}}$) in the Frontal Cordillera foothills and Iglesia Basin, and highest ($>3.0\ \mathrm{mm\,yr^{-1}}$) in the Eastern Precordillera triangle zone since 3 Ma (Fig. 6). Moreover, AHe thermochronology of the Miocene Huaco section yields some of the youngest reported dates observed in the foreland region compared to pre-Cenozoic data within this sector of the Andean retroarc region (e.g., Dávila and Carter, 2013 and references therein). This finding suggests the thermal conditions in the Huaco area during basin burial were sufficiently hot to reset Miocene detrital apatite and point to more complex (e.g., higher) Neogene geothermal gradient variations across the Andean foreland region than previously considered.

Taken together, calculated erosion rates from thermochronometric data indicate that the highest erosion rates are present along the margins of the Iglesia basin in the west and in the easternmost toe of the Eastern Precordillera. The synchroneity between deformation and erosion along the tectonically active boundaries

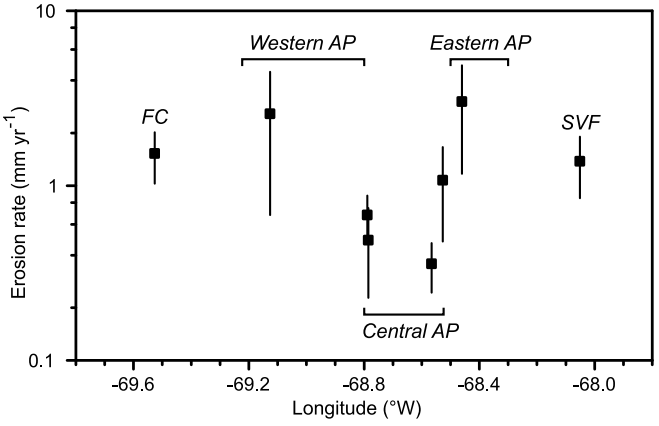

Fig. 6. Long-term erosion rates across the Precordillera and adjacent provinces, estimated from inversion of apatite (U–Th)/He thermochronometric ages following method of Willett and Brandon (2013). Highest erosion rates are observed along the structural boundaries of the Precordillera – in the Frontal Cordillera and Western Precordillera and Eastern Precordillera triangle zone.

of the Precordillera (this study), and flattening of the Nazca plate beneath the region (Kay et al., 2005; Ramos et al., 2002) suggest that erosional processes responded to deformation and changes in stress conditions in the foreland region. Notably, deformation styles within these margins of the Precordillera depart from purely orthogonal deformation and exhibit sinistral transpression (in the west) and strike-slip faulting and involvement of basement structures (in the east) that may be a manifestation of stresses transferred to the upper plate by flat slab subduction (e.g., Japas et al., 2015; Siame et al., 2005).

This long-term deformation and unroofing history is compatible with Quaternary faulting and seismicity patterns. For instance, Quaternary thrust fault scarps along the Niquivil thrust are described in the eastern toe of the Central Precordillera (Allmendinger and Judge, 2014), and the Pleistocene strike-slip El Tigre fault (Bastías and Bastías, 1987) and other fault scarps in the Iglesia Basin (Alvarez-Marrón et al., 2006) indicate active deformation to the west of the Precordillera. There is generally a high rate of seismicity in the Cuyania terrane (e.g., Alvarado et al., 2007), and 30°S latitude, and most seismicity is concentrated beneath the eastern toe of the Central Precordillera, the Eastern Precordillera, and the terrane boundary with the Sierras Pampeanas (Siame et al., 2005; Smalley et al., 1993). We note that geodetic measurements show no changes strain gradient across the Iglesia Basin, whereas there is a decrease in strain rate observed across the structural boundary between the Eastern Precordillera and the Sierras Pampeanas (Allmendinger and Judge, 2014; Brooks et al., 2003).

4.2. Basin provenance record of thrust belt deformation and exhumation

Eastward directed paleoflow indicators point to the Precordillera and the Frontal Cordillera as primary contributors of sediment for the Bermejo Basin, although the relative proportions of Precordillera versus Frontal Cordillera contribution has been difficult to quantify in the past (e.g., Jordan et al., 1993). Dominant lithologic types in the Frontal Cordillera are mostly volcanic and plutonic rocks, whereas the Precordillera consists of marine to continental metasedimentary rocks. Our detrital zircon geochronological data complements existing provenance information and illuminates the evolution of source areas that provided sediment to the Bermejo Basin (Fig. 5). We categorize the analyzed zircons from the Miocene basin infill at Huaco into five major U–Pb age populations that are representatives of primary igneous sources and potential recycled sedimentary units in Paleozoic–Mesozoic strata (Fig. 5):

(1) **Late Jurassic – Miocene granitoids and volcanic rocks of the Andean magmatic arc** are presently located in the coast range of Chile. These source rocks include the Jurassic Panguipulli batholith (180–160 Ma), the Paleogene Cogotí group (64–38 Ma), and Neogene plutons that young eastward across the arc from 27–18 Ma to 7–0 Ma (Parada, 1990). Spatiotemporal migration of Neogene magmatism reflects progressive shallowing of the Pampean flat slab and cessation of arc magmatism (e.g., Kay et al., 2005; Ramos et al., 2002).

(2) **Permo-Triassic Choiyoi igneous province** that consists of 230–280 Ma granitoids and silicic volcanics that formed during intraplate extension and magmatism (Mpodozis and Kay, 1992). The Choiyoi Group and associated rift basins are exposed across a broad area of western Argentina including the Frontal Cordillera, the San Rafael block, and the Main Cordillera.

(3) **Pre-Choiyoi Carboniferous – Permian Chilean batholiths** include 290–330 Ma calc-alkaline granitoid plutons exposed in the Frontal Cordillera and Main Cordillera (Mpodozis and Kay, 1992). These igneous units include the 290–310 Ma Elqui Complex and intra-arc basins in Chile and the Colangüil batholith. The Late Carboniferous Coastal Batholith of Chile is another potential primary igneous source for zircons of this age range. We note that Carboniferous–Permian zircons are a dominant component of sediment in the Paleozoic accretionary basins in Chile (Bahlburg et al., 2009).

(4) **Sierras Pampeanas magmatic arcs and crystalline orogens** include the Carboniferous post-orogenic granites in the Sierra del Velasco (330–360 Ma; Grosse et al., 2009), the Ordovician Famatinian arc (460–495 Ma; Ducea et al., 2010); the Cambrian Pampean arc (525–550 Ma) and other Neoproterozoic rocks (525–600 Ma) of the Eastern Sierras Pampeanas orogens and Brasiliano belts (Ramos, 2009). Pampean zircons are also present in the Paleozoic accretionary basins in Chile (Bahlburg et al., 2009) and the Cambrian–Ordovician strata in the Precordillera (Finney et al., 2005; Gleason et al., 2007).

(5) **Proterozoic zircon sources** include the Late Mesoproterozoic – early Neoproterozoic the Cuyania Grenvillian basement beneath the Precordillera (900–1200 Ma; Ramos, 2004), the Sunsás magmatic belt 900–1200 Ma, and various Amazonia cratonic blocks (Bahlburg et al., 2009). Paleoproterozoic crystalline sources include the Río de la Plata Craton and associated Amazon cratonic sources in eastern Argentina (Ramos, 2009) and Neoproterozoic Brasiliano belts. Zircons of these ages are reported in the Paleozoic accretionary basins in Chile (Bahlburg et al., 2009) and the Cambrian–Ordovician strata in the Precordillera (Finney et al., 2005; Gleason et al., 2007).

In the following section, we highlight the important patterns and upsection trends in these major detrital zircon U–Pb age populations. First, there is general similarity between detrital signatures from the Quebrada del Jarillal Fm. (ca. 16–12.4 Ma). The noticeable upsection increase in the Permo-Triassic Choiyoi population likely reflects the added contribution of sediment derived from the Frontal Cordillera (Fig. 5B), consistent with high percentage of lithic volcanic grains in the basin infill (Jordan et al., 1993). We also note that the detrital zircon signature of the lower Quebrada del Jarillal Fm. is strikingly similar to the Permian Chilean accretionary basins (Bahlburg et al., 2009) and Lower Permian Patquía Fm. in the Precordillera (this study), all of which contain prominent Carboniferous–Permian zircons ca. 390–320 Ma and similar Sierras Pampeanas and Sunsás/Grenvillian zircon populations (compare pink to bold gray and bold black lines in Fig. 5A). To-

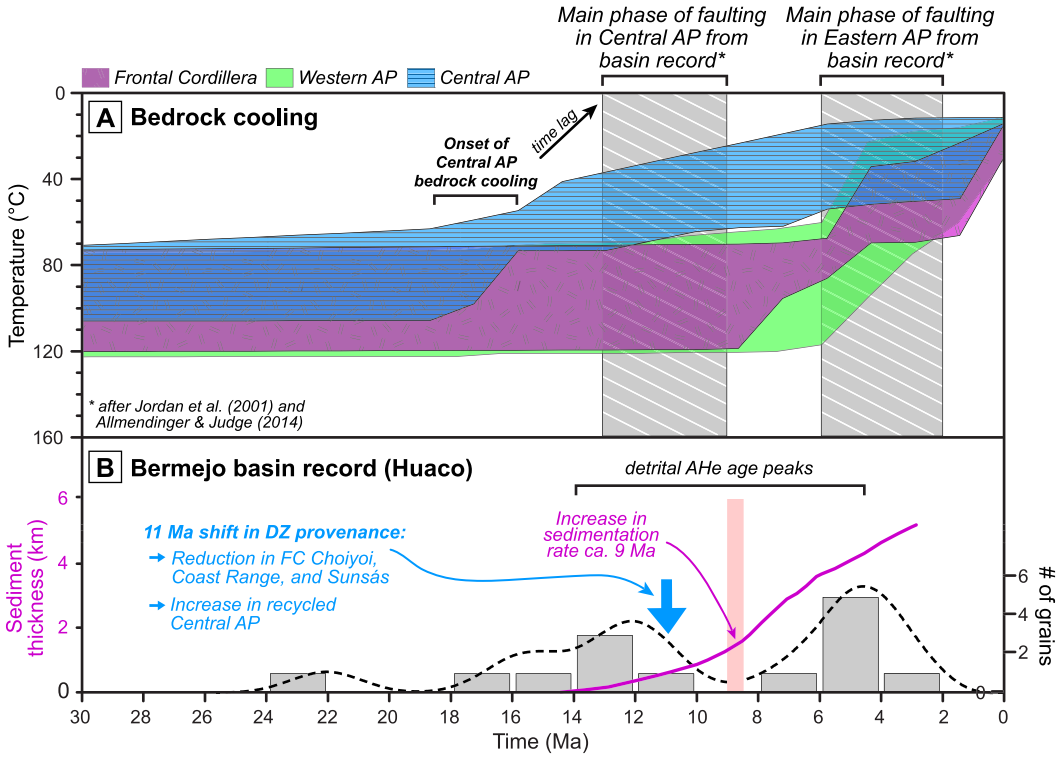

Fig. 7. Summary of bedrock cooling models, faulting chronology, and basin sedimentation history. A) T–t windows for good-fit HeFTy inverse model results for the Frontal Cordillera, Western Precordillera, and Central Precordillera since 30 Ma. Light gray hatched windows indicate duration of main phase of thrusting in the Central and Eastern Precordillera (Allmendinger and Judge, 2014; Jordan et al., 2001). B) Sediment accumulation curve (magenta line) from Jordan et al. (2001), showing increase in sedimentation rate ca. 9 Ma. Blue arrow indicates timing of provenance shift observed in detrital zircon geochronology data toward increased Precordillera sources. Black dashed line shows relative probability distribution of detrital AHe dates (also shown by gray histogram) from the Río Jáchal Formation. (For interpretation of the references to color in this figure legend, the reader is referred to the web version of this article.)

gether, with the presence of Paleogene Andean arc zircons, these findings support fluvial connectivity through the Frontal Cordillera to the Main Cordillera and Chilean coastal range during deposition of the Quebrada del Jarillal Fm.

The most important shift in sediment provenance occurs between 12.4 and 9.6 Ma: the Permo-Triassic Choiyoi population decreases substantially, whereas the Carboniferous–Permian peak dominates the detrital signature from 9.6–8.1 Ma. Over this transition, the proportion of Pampean zircons increases (blue and green lines in Fig. 5A), whereas the Grenvillian/Sunsás zircons and Cenozoic Andean arc populations decrease. In comparison to the detrital zircon signature of the Cambrian–Ordovician strata in the Precordillera, which is dominated by Mesoproterozoic and Neoproterozoic grains (red line, Fig. 5A), we suggest that the upsection increase in the Sierras Pampeanas grains can be explained by added sediment contribution from the Precordillera due to unroofing of the lower Paleozoic strata in the Central Precordillera by 9.6 Ma (i.e., compare zircon signatures of the Cambro-Ordovician formations from Finney et al., 2005 and Gleason et al., 2007). The detrital zircon U–Pb results are consistent with the appearance of limestone clasts and an increase in lithic sedimentary grains at ca. 10 Ma that represent the earliest surface exposure and faulting of Cambro-Ordovician strata in the Central Precordillera (Jordan et al., 1993). Detrital studies farther south in the Precordillera intermontane basins near San Juan (Fig. 1) record a slightly earlier sediment provenance shift to predominantly Precordillera source areas at ca. 14–12 Ma, based on upsection increasing trends in sedimentary clasts and zircon U–Pb geochronology (Levina et al., 2014).

Previous workers have characterized this change in provenance to correspond to a change in basin paleodrainage from throughgoing streams to more distributary channel system interpreted as a consequence of uplift of the Central Precordillera and formation of an extensive mountainous area in the Precordillera (Jordan et al., 2001). Our findings support the interpretation of a mountainous Precordillera region and further suggest that the Frontal Cordillera provided relatively little sediment input from 9.6 and 8.1 Ma, based on the paucity of Choiyoi Group zircons. Furthermore, a comparison between long-term erosion rates (0.33–0.49 mm yr^{-1}) of the Central Precordillera and sediment accumulation rates (~0.30 mm yr^{-1}; Jordan et al., 2001) at Huaco during Middle Miocene time indicates a first-order balance between erosion and sediment accumulation. By 2 Ma, however, a renewed sediment input from the volcanic-rich Frontal Cordillera is evident in the Mogna Formation (Johnson et al., 1986).

4.3. Time lag between bedrock cooling and sedimentary signals of faulting

Changes in sedimentary provenance and detrital thermochronological signatures are widely used to decipher the timing and rates of deformation, and over Myr timescales, time lags between faulting, surface uplift, erosion and deposition (e.g., Burbank, 2002). However, given the pervasive challenge of directly dating fault motion, few studies are able to quantify the lag times between bedrock cooling and erosion. We find that bedrock cooling across the Central Precordillera commenced between 18–14 Ma – as much as 2–6 Myr prior to changes in sedimentary provenance from the basin record (Fig. 7). This finding implies that lateral heat advection and rock cooling occurs during construction of topography, as suggested in other studies (Ehlers and Farley, 2003), of the Central Precordillera thrust faults, particularly the Blanco Thrust, which in turn was followed by erosion during continued thrusting.

Specifically to the Bermejo Basin, Jordan et al. (1993) noted some degree of uncertainty on the timing of faulting constrained

by provenance proxies because of the potential for a time delay between faulting and surface exposure of the Cambro-Ordovician limestone in the Central Precordillera thrust sheets. In tectonically active settings within semi-arid environments, we suggest that, bedrock cooling is a more sensitive measure of the onset of faulting (via lateral cooling), followed by erosion of uplifted hanging-wall blocks. Since bedrock cooling histories are difficult to relate to a single thrust, the added presence of exceptionally well-preserved growth strata and unconformable relationships in the Precordillera together with our new data provide a more complete record of tectonics.

Finally, we highlight the internal consistency in detrital records and note that important shifts in both the detrital zircon geochronology (i.e., reduction in Choiyoi and increase in recycled Paleozoic grains) and modal sandstone composition (i.e., increase in sedimentary lithic grains; Jordan et al., 1993) both rigorously record the timing of major source area reorganization at ca. 10 Ma. In light of paleoaltimetry constraints of surface uplift of the Precordillera after 10 Ma (Hoke et al., 2014a) and pronounced cooling at ca. 10 Ma from detrital thermochronology (Levina et al., 2014) in the southern Precordillera, we suggest that the 2–6 Myr lag time between bedrock cooling (this study), surface uplift, and the detrital records reflects the time necessary to build sufficient Precordillera topography and cause a major physiographic change in upland source areas during the latest Miocene–Pliocene.

5. Conclusions

Low-temperature thermochronology from the Argentine Precordillera highlight eastward migration of the erosional front during in-sequence structural growth between 18 Ma and 2 Ma. Most rapid denudation corresponds to areas of most recent (Pliocene–Quaternary) faulting, concentrated along the structural extremities of the Precordillera, specifically in the foothills of the Frontal Cordillera and within the Eastern Precordillera triangle zone. Detrital zircon geochronology from the Bermejo Basin at Huaco provides more detailed provenance information on source drainage reorganization at ca. 10 Ma. Specifically, our findings document igneous sources from the Frontal Cordillera as well as connection to external sediment sources in the Main Cordillera and possibly the Chilean Coast Range from 16–14 Ma. Between 12.4–9.6 Ma, detrital geochronology reveals an important eastward shift in provenance to the Precordillera and substantial reduction of sediment derived from the Frontal Cordillera. By 9.6 Ma, the Precordillera was the primary contributor of sediment to the Bermejo Basin at Huaco and persisted as such until Pliocene time. The bedrock cooling history of the Central Precordillera suggests 2–6 Myr earlier onset of faulting compared to previous chronology of deformation, suggesting a time lag between bedrock cooling related to faulting and the appearance of these tectonic signals in the detrital foreland basin record.

Lastly, we suggest that increased erosion along the flanks of the Precordillera was coeval with Pliocene out-of-sequence faulting and basement faulting in the Sierras Pampeanas, which together are likely a deformational response to changes in stress conditions during Pampean flat subduction. In this view, reactivation of basement structures and terrane boundaries (e.g., Ramos et al., 2002) beneath the Eastern Precordillera and the Iglesia Basin may be responsible for concentrating stress above the Pampean flat-slab, enhancing erosion. Similar spatial patterns of deformation have been observed in the Principal Cordillera hinterland, where out-of-sequence faulting and reactivation of older structures in the Aconcagua fold-and-thrust belt has been linked to flat slab subduction (Ramos, 2009; Ramos et al., 2002). Moreover, high erosion rates in the Frontal Cordillera point to a hinterland shift in locus of erosion since Pliocene time, which may be a previously unrecognized signal of out-of-sequence deformation and changing kinematics during flat-slab subduction.

Acknowledgements

We greatly acknowledge fruitful discussions on Andean geology with P. Alvarado, A. Stevens, G. Hoke, P. Val, T. Jordan, and B. Horton. We thank T. Jordan for advice on sampling strategy in the Huaco section. C. Painter, S. Thomson, and P. Reiners generously provided assistance in the Arizona Radiogenic Helium Dating Laboratory and Arizona Fission Track Laboratory. We also thank M. Pecha, N. Giesler, and other laboratory personnel for analytical assistance in the LaserChron Center. Constructive comments from R. Allmendinger and V. Ramos greatly contributed to the scope and clarity of the manuscript. This research was supported by U.S. National Science Foundation grant EAR-1049605 awarded to JCF.

Appendix A. Supplementary material

Supplementary material related to this article can be found online at http://dx.doi.org/10.1016/j.epsl.2015.09.041.

References

Allmendinger, R.W., Figueroa, D., Snyder, D., Mpodozis, C., Isacks, L., 1990. Foreland shortening and crustal balancing in the Andes at 30°S latitude. Tectonics 9, 789–809.

Allmendinger, R.W., Judge, P.A., 2014. The Argentine Precordillera: a foreland thrust belt proximal to the subducted plate. Geosphere 10 (6), 1203–1218.

Alonso, J.L., Gallastegui, J., Rodríguez Fernández, L.R., García-Sansegundo, J., 2014. Stratigraphy and structure of the Punta Negra Anticline. Implications on the structural evolution of the Argentine Precordillera. J. Iber. Geol. 40, 283–292.

Alvarado, P., Beck, S., Zandt, G., 2007. Crustal structure of the south-central Andes Cordillera and backarc region from regional waveform modelling. Geophys. J. Int. 170, 858–875.

Alvarez-Marrón, J., Rodríguez-Fernández, R., Heredia, N., Busquets, P., Colombo, F., Brown, D., 2006. Neogene structures overprinting Palaeozoic thrust systems in the Andean Precordillera at 30°S latitude. J. Geol. Soc. Lond. 163, 949–964.

Bahlburg, H., Vervoort, J.D., Du Frane, S.A., Bock, B., Augustsson, C., Reimann, C., 2009. Timing of crust formation and recycling in accretionary orogens: insights learned from the western margin of South America. Earth-Sci. Rev. 97, 215–241.

Bastías, H.E., Bastías, J.A., 1987. Fallamiento rumbo-deslizante en el borde oriental de los Andes entre los 32 y 26 grados de latitud sur. In: X Congreso Geológico Argentino Actas, pp. 207–210.

Beaumont, C., Fullsack, P., Hamilton, J., 1992. Erosional control of active compressional orogens. In: McClay, K.R. (Ed.), Thrust Tectonics. Chapman and Hall, pp. 1–18.

Beer, J.A., Allmendinger, R.W., Figueroa, D.E., Jordan, T.E., 1990. Seismic stratigraphy of a Neogene piggyback basin, Argentina. Am. Assoc. Pet. Geol. Bull. 74, 1183–1202.

Brooks, B.A., Bevis, M., Smalley, R.J., Kendrick, E., Manceda, R., Lauría, E., Maturana, R., Araujo, M., 2003. Crustal motion in the Southern Andes (26°–36°S): do the Andes behave like a microplate? Geochem. Geophys. Geosyst. 4, 1–14.

Burbank, D.W., 2002. Rates of erosion and their implications for exhumation. Mineral. Mag. 66, 25–52.

Cahill, T., Isacks, B.L., 1992. Seismicity and shape of the subducted Nazca Plate. J. Geophys. Res. 97, 17503. http://dx.doi.org/10.1029/92JB00493.

Cande, S.C., Kent, D.V., 1995. Revised calibration of the geomagnetic polarity timescale for the Late Cretaceous and Cenozoic. J. Geophys. Res. 100, 6093–6095.

Dávila, F.M., Carter, A., 2013. Exhumation history of the Andean broken foreland revisited. Geology 41, 443–446.

Davis, D., Suppe, J., Dahlen, F.A., 1983. Mechanics of fold-and-thrust belts and accretionary wedges. J. Geophys. Res. 88, 1153–1172.

Ducea, M.N., Otamendi, J.E., Bergantz, G., Stair, K.M., Valencia, V.a., Gehrels, G.E., 2010. Timing constraints on building an intermediate plutonic arc crustal section: U–Pb zircon geochronology of the Sierra Valle Fértil–La Huerta, Famatinian arc, Argentina. Tectonics 29. http://dx.doi.org/10.1029/2009TC002615.

Ehlers, T.A., Farley, K.A., 2003. Apatite (U–Th)/He thermochronometry: methods and applications to problems in tectonic and surface processes. Earth Planet. Sci. Lett. 206, 1–14.

Finney, S., Peralta, S., Gehrels, G.E., Marsaglia, K., 2005. The Early Paleozoic history of the Cuyania (greater Precordillera) terrane of western Argentina: evidence from geochronology of detrital zircons from Middle Cambrian sandstones. Geol. Acta 3, 339–354.

Furque, G., González, P.D., Caballé, M.F., 2003. Hoja Geológica 3169—II San José de Jáchal, 1:250,000. SEGEMAR Inst. Geol. y Recur. Miner., vol. 259, pp. 1–83.
Gleason, J.D., Finney, S.C., Peralta, S.H., Gehrels, G.E., Marsaglia, K.M., 2007. Zircon and whole-rock Nd–Pb isotopic provenance of Middle and Upper Ordovician siliciclastic rocks, Argentine Precordillera. Sedimentology 54, 107–136.
Green, P.F., Duddy, I.R., Laslett, G.M., Hegarty, K.A., Gleadow, A.J.W., Lovering, J.F., 1989. Thermal annealing of fission tracks in apatite: 4. Quantitative modeling techniques and extension to geological time scales. Chem. Geol. 79, 155–182.
Grosse, P., Söllner, F., Báez, M.A., Toselli, A.I., Rossi, J.N., de la Rosa, J.D., 2009. Lower Carboniferous post-orogenic granites in central eastern Sierra de Velasco, Sierras Pampeanas, Argentina: U–Pb monazite geochronology, geochemistry and Sr–Nd isotopes. Int. J. Earth Sci. 98, 1001–1025.
Gutscher, M.-A., Spakman, W., Bijwaard, H., Engdahl, E.R., 2000. Geodynamics of flat subduction: seismicity and tomographic constraints from the Andean margin. Tectonics 19, 814–833.
Hilley, G.E., Blisniuk, P.M., Strecker, M.R., 2005. Mechanics and erosion of basement-cored uplift provinces. J. Geophys. Res. 110, 1–22.
Hoke, G.D., Giambiagi, L.B., Garzione, C.N., Mahoney, J.B., Strecker, M.R., 2014a. Neogene paleoelevation of intermontane basins in a narrow, compressional mountain range, southern Central Andes of Argentina. Earth Planet. Sci. Lett. 406, 153–164.
Hoke, G.D., Graber, N.R., Mescua, J.F., Giambiagi, L.B., Fitzgerald, P.G., Metcalf, J.R., 2014b. Near pure surface uplift of the Argentine Frontal Cordillera: insights from (U–Th)/He thermochronometry and geomorphic analysis. Geol. Soc. (Lond.) Spec. Publ. 399. http://dx.doi.org/10.1144/SP399.4.
Japas, M.S., Re, G.H., Oriolo, S., Vilas, J.F., 2015. Palaeomagnetic data from the Precordillera fold and thrust belt constraining Neogene foreland evolution of the Pampean flat-slab segment (Central Andes, Argentina). Geol. Soc. (Lond.) Spec. Publ. 425. http://dx.doi.org/10.1144/SP425.9.
Johnson, N.M., Jordan, T.E., Johnnson, P.A., Naeser, C.W., 1986. Magnetic polarity stratigraphy, age and tectonic setting of fluvial sediments in an eastern Andean foreland basin, San Juan Province, Argentina. Spec. Publ. Int. Assoc. Sedimentol. 8, 63–75.
Jordan, T.E., Allmendinger, R.W., 1986. The Sierras Pampeanas of Argentina: a modern analogue of Rocky Mountain foreland deformation. Am. J. Sci. 286, 737–764.
Jordan, T.E., Allmendinger, R.W., Damanti, J.F., Drake, R.E., 1993. Chronology of motion in a complete thrust belt: the Precordillera, 30–31°S, Andes Mountains. J. Geol. 101, 135–156.
Jordan, T.E., Schlunegger, F., Cardozo, N., 2001. Unsteady and spatially variable evolution of the Neogene Andean Bermejo foreland basin, Argentina. J. South Am. Earth Sci. 14, 775–798.
Kay, S.M., Godoy, E., Kurtz, A., 2005. Episodic arc migration, crustal thickening, subduction erosion, and magmatism in the south-central Andes. Geol. Soc. Am. Bull. 117, 67–88.
Ketcham, R.A., 2005. Forward and inverse modeling of low-temperature thermochronometry data. Rev. Mineral. Geochem. 58, 275–314. http://dx.doi.org/10.2138/rmg.2005.58.11.
Koons, P., Kirby, E., 2007. Topography, denudation, and deformation: the role of surface processes in fault evolution. In: Handy, M.R., Hirth, G., Hovius, N. (Eds.), Tectonic Faults: Agents of Change on a Dynamic Earth. MIT Press, Cambridge, MA, pp. 205–230.
Levina, M., Horton, B.K., Fuentes, F., Stockli, D.F., 2014. Cenozoic sedimentation and exhumation of the foreland basin system preserved in the Precordillera thrust belt (31–32°S), southern central Andes, Argentina. Tectonics 33 (9). http://dx.doi.org/10.1002/2013TC003424.
Lock, J., Willett, S., 2008. Low-temperature thermochronometric ages in fold-and-thrust belts. Tectonophysics 456, 147–162.
Mpodozis, C., Kay, S.M., 1992. Late Paleozoic to Triassic evolution of the Gondwana margin: evidence from Chilean Frontal cordilleran batholiths (28°S to 31°S). Geol. Soc. Am. Bull. 104, 999–1014.
Ortíz, G., Alvarado, P., Fosdick, J.C., Perucca, L., Saez, M., Venerdini, A., in press. Active deformation in the northern Sierra de Valle Fértil, Sierras Pampeanas, Argentina. J. South Am. Earth Sci. http://dx.doi.org/10.1016/j.jsames.2015.08.015.
Parada, M.A., 1990. Granitoid plutonism in central Chile and its geodynamic implications; a review. Spec. Pap., Geol. Soc. Am. 241.
Ramos, V.A., 2009. Anatomy and global context of the Andes: main geologic features and the Andean orogenic cycle. Mem. Geol. Soc. Amer. 204, 31–65.
Ramos, V.A., 2004. Cuyania, an exotic block to Gondwana: review of a historical success and the present problems. Gondwana Res. 7, 1–18.
Ramos, V.A., Cristallini, E.O., Pérez, D.J., 2002. The Pampean flat-slab of the Central Andes. J. South Am. Earth Sci. 15, 59–78.
Reiners, P.W., Brandon, M.T., 2006. Using thermochronology to understand orogenic erosion. Annu. Rev. Earth Planet. Sci. 34, 419–466.
Siame, L.L., Bellier, O., Sébrier, M., Araujo, M., 2005. Deformation partitioning in flat subduction setting: case of the Andean foreland of western Argentina (28°S–33°S). Tectonics 24. http://dx.doi.org/10.1029/2005TC001787.
Smalley, J.R., Pujol, J., Regnier, M., Chiu, J.-M., Chatelain, J.-L., Isacks, B.L., Araujo, M., Puebla, N., 1993. Basement seismicity beneath the Andean precordillera thin-skinned thrust belt and implications for crustal and lithospheric behavior. Tectonics 12, 63–76.
Vergés, J., Ramos, V.A., Meigs, A., Cristallini, E.O., Bettini, F.H., Cortés, J.M., 2007. Crustal wedging triggering recent deformation in the Andean thrust front between 31°S and 33°S: Sierras Pampeanas–Precordillera interaction. J. Geophys. Res. 112, B03S15. http://dx.doi.org/10.1029/2006JB004287.
Willett, S.D., Brandon, M.T., 2013. Some analytical methods for converting thermochronometric age to erosion rate Sean. Geochem. Geophys. Geosyst. 14, 209–222.
Yañez, G.A., Ranero, C.R., von Huene, R., Díaz, J., 2001. Magnetic anomaly interpretation across the southern central Andes (32°–34°S): the role of the Juan Fernández Ridge in the late Tertiary evolution of the margin. J. Geophys. Res. 106, 6325–6345.
Zapata, T.R., Allmendinger, R.W., 1996. Growth stratal records of instantaneous and progressive limb rotation in the Precordillera thrust belt and Bermejo basin, Argentina. Tectonics 15, 1065–1083.